Available online at www.sciencedirect.com

ScienceDirect

Procedia CIRP 111 (2022) 271–276

www.elsevier.com/locate/procedia

12th CIRP Conference on Photonic Technologies [LANE 2022], 4-8 September 2022, Fürth, Germany

Effect of DED process parameters on distortion and residual stress state of additively manufactured Ti-6Al-4V components during machining

Denys Romanenko[a,*], Vishnuu Jothi Prakash[b], Tobias Kuhn[a], Carsten Moeller[a], Wolfgang Hintze[a], Claus Emmelmann[c]

[a]*Hamburg University of Technology, Institute of Production Management and Technology, Denickestraße 17, 21073 Hamburg, Germany*
[b]*Fraunhofer Research Institution for Additive Manufacturing Technologies IAPT, Am Schleusengraben 14, 21029 Hamburg, Germany*
[c]*Hamburg University of Technology, Institute of Laser and System Technologies, Harburger Schloßstraße 28, Channel 4, 21079 Hamburg, Germany*

* Corresponding author. Tel.: +49-40-42878-4132. *E-mail address:* denys.romanenko@tuhh.de

Abstract

One of the major challenges in high-deposition rate Directed Energy Deposition processes is the resultant residual stresses generated during material deposition, often leading to distortion and poor material characteristics. Important part families suitable for DED process in aerospace sector are thin-wall components, characterized by a large base surface area with rib-like strengthening structures. Here, the substrate plate can be designed to be a part of the final component. The integration of substrate plate into final component results in possible deformation due to residual stress release during machining. This paper therefore investigates the effect of various powder-based Laser Metal Deposition process parameters and strategies on the residual stress state of the additively manufactured Ti-6Al-4V components and the resulting stress release during machining process. The analysis has been carried out during the machining process by including in-process strain measurements of the substrate. The embraced layer removal method allows the determination of machining zone specific stress release mapping, based on an analytical and FEM-model. Hence, the initial residual stress state of the builds was calculated, which revealed that although the heat treatment resolved most of the residual stresses, also in heat treated parts residues were identified depending on the part clamping during the treatment. Furthermore, the study revealed that the significant residual stresses are present in the layers close to the substrate.

Keywords: Directed Energy Deposition; Residual Stresses; Distortion; Process Parameters; Machining Strategies.

1. Introduction

Directed Energy Deposition (DED) technique, a classification of Additive Manufacturing (AM) technology, is known for its characteristic high deposition rate and large build volume. Laser Metal Deposition (LMD) process, a sub-classification of DED technology, employs focused laser beam as an energy source for layer-wise deposition resulting in a minimalistic heat affected zone, making this process one of the most favorable and widely employed DED technologies. In addition to repair applications and prototype development, efforts have been seen in industrialization of this technology for serial production of aerospace components [1]. Being a resource efficient manufacturing process, components with higher buy-to-fly ratios when manufactured conventionally, like machining from a block, are usually chosen for fabrication through LMD process. This near-net shape process, however, requires a mandatory final machining step to obtain a functional component. Thin-wall components which are characterized by a large base surface area with rib-like strengthening structures are one of the most suitable part families for DED technology.

One of the major challenges in DED technique, that hinders wide-spread industrialization, are the resultant residual stresses that manifest into distortion, delamination and hot cracking, during or in the downstream machining process [2, 3]. Various

10.1016/j.procir.2022.08.020

process parameters and strategies are tailored during the deposition process to minimize distortion and to eliminate defects. These process parameters and strategies, however, can have adverse or useful effects in the mandatory downstream machining process. This paper, therefore, investigates the effects of such tailored process parameters and strategies on the residual stress state and distortion of additively manufactured Ti-6Al-4V components during machining. For this, the generated layers are machined while detecting in-process strain and post-process deflection of the builds. The results are used as input for analytical and FEM-based reversed calculation of the initial residual stresses. In contrast to most of the papers, where the residual stresses are obtained through contour, hole drilling and x-ray/neutron diffraction [4], here the link between DED-process, through the machining induced part deflection and the initial residual stress state is made.

Nomenclature

a_e	work intervention at milling	[mm]
a_p	depth of cut	[mm]
Bk	Build number k	[-]
b	substrate width	[mm]
d	deposit thickness	[mm]
$e_{1.i}$	span build top/neutral plane	[mm]
$e_{2.i}$	span substrate bottom/neutral plane	[mm]
$F_{i,eq}$	equivalent forces at stress release	[N]
F_f	feed force	[N]
F_{fN}	feed normal force	[N]
F_P	passive force	[N]
h	initial height deposit	[mm]
h_i	deposit height after removal of layer i	[mm]
hm	middle deposit height in layer i	[mm]
I_{xx}	second moment of area	[mm^4]
i	number of removed layer	[-]
j	number of considered layer	[-]
l	initial length deposit	[mm]
l_s	substrate length	[mm]
s_i	height of layer i	[mm]
t	substrate thickness	[mm]
w	deflection indicator in the yz-plane	[mm]
x, y, z	cartesian coordinates	[mm]
$S_{1,i}$	stress build top after removing layer i	[MPa]
$S_{2,i}$	stress substrate bottom after removing layer i	[MPa]
$S_{y,i,j}$	additionally induced avg. stress in layer j after removal of layer i	[MPa]
α	deflection indicator in the yz-plane	[°]
ε_i	strain at build bottom after removal of layer i	[-]
$\sigma_{m,i}$	mean residual stress in layer i before removal	[MPa]
$\sigma_{x,y,z}$	stress in x/y/z-direction	[MPa]
$\sigma_{y,j}$	avg. residual stress in y-direction in layer j	[MPa]
$\sigma_{y,i,j}$	avg. σ_y in layer j after removal of layer i	[MPa]

2. Residual stresses and its mitigation in DED

Any DED process undergoes rapid heating of substrate and material (powder or wire) during deposition, followed by rapid cooling of the deposited layer. The rapid heating-cooling thermal cycle of top-layers and partial re-melting of underlying pre-built layers in a layer-wise manner leads to formation of residual stresses in the component [2, 5].

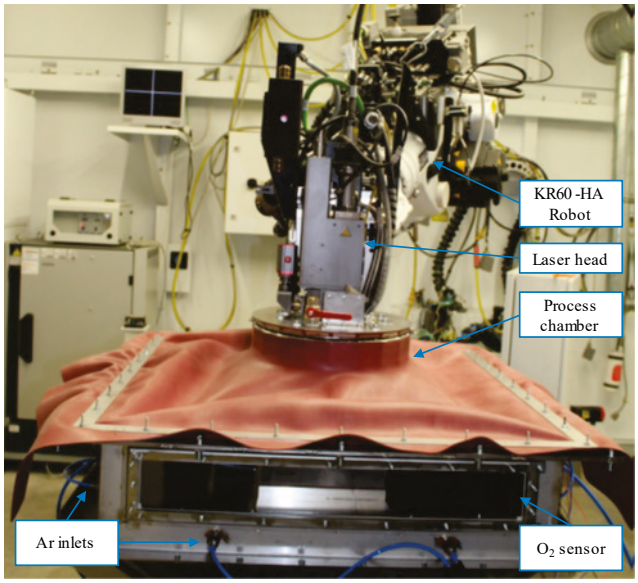

Fig. 1. Experimental setup for fabrication of test samples.

Several research works have focused on mitigation of adverse effects of residual stresses through optimization of process parameters like laser power, deposition velocity, deposition strategy and inter-layer waiting time to achieve a controlled thermal gradient [6, 7]. Other process strategies to minimize residual stresses in DED processes include substrate design, build geometry change, substrate pre-heating, laser shock peening and heat treatment including intermittent stress-relief heat treatment [8, 9, 10].

Unlike Powder Bed Fusion process, in DED process, the substrate is in many cases integrated into the final design of the component. This eliminates the intermediate wire-cut EDM process that is employed to remove additively fabricated component from the substrate plate. During this process, the resultant residual stresses will be released, but induce additional part deformation. However, when substrate is integrated into final geometry, this process step will be eliminated, and the resultant residual stresses will be mitigated during the machining process.

Thermo-mechanical simulation-based and analytical modelling of the induced residual stresses during the generative and subtractive process is the subject of current research [11 - 16]. However, the link between the variation of DED process parameters, the machining of the builds and the reversed determination of the residual stress state of the parts is not sufficiently investigated so far. The required experimental work has been conducted in this paper and supported through analytical and simulation-based models.

3. Experimental procedure

3.1. DED manufacturing setup and material

Test samples for analysis of distortion and residual stress state were manufactured using a Laser Metal Deposition system from *TRUMPF SE + Co. KG*. Fig. 1 shows the

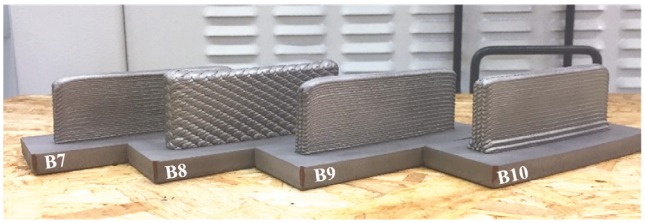

Fig. 2. Fabricated test samples.

machine setup along with a shielding gas process chamber used for fabrication of reactive materials like Ti-6Al-4V, as in this case. The system setup consists of a three-nozzle deposition head with a powder feeder system attached to a 6-axis industrial robot. The laser source is a 6 kW multi-mode continuous Yb-YAG disk laser with a wavelength of 1.03 µm. The in-house developed shielding chamber was flooded with Ar gas at 60 lpm during deposition to achieve O_2 level <150 ppm. The material chosen was Ti-6Al-4V Grade 5 in powder form with a particle distribution of 45 - 105 µm. The substrate procured had the same material composition.

3.2. DED process parameters, process strategies and experimental plan

Table 1. Description and experimental conditions for build jobs

Build job	Substrate pre-heating	Deposition strategy	Dwell time	Heat treatment (condition)
B1	No	Length-wise	0	No
B2	Yes	Length-wise	0	Yes (not clamped)
B3	No	Length-wise	0	Yes (clamped)
B4	Yes	Length-wise	0	Yes (clamped)
B5	No	Length-wise	0	Yes (clamped)
B6	No	Length-wise	0	Yes (clamped)
B7	No	Length-wise	0	Yes (not clamped)
B8	No	Cross-wise (45˚)	0	Yes (not clamped)
B9	No	Length-wise	10 s	Yes (not clamped)
B10	No	Geometry change	0	Yes (not clamped)

Primary process parameters employed in laser metal deposition process are laser power, deposition velocity and material flow rate. Several research works have focused on optimization of these parameters and studied their effect on residual stress states and distortion. Hence, in this paper, an optimized primary process parameter set has been taken and the effects of some of the secondary process parameters or strategies have been studied. These include deposition

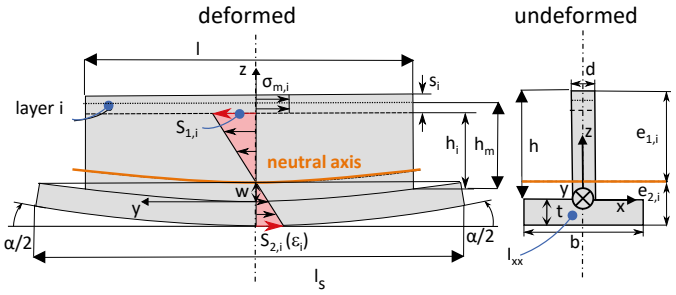

Fig. 3. Geometrical properties, removed material layer i, stress shift and deformation of the builds.

- with or without substrate pre-heating of the substrate up to 300 ˚C
- with deposition strategy variation (length-, cross-wise)
- with or without inter-layer dwell time
- with or without heat treatment as per AMS 2801
- with or without clamping tool during heat treatment

The experimental plan can be seen in Table 1. The fabricated wall geometry had a build dimension of 100 mm x 35 mm x 9.5 mm (l x h x d) built over a 130 mm x 46 mm x 10 mm (l_s x b x t) substrate plate. The samples were fabricated with 1450 W laser power, at 0.01 m/s and at a deposition rate of about 120 cm^3/h. Some of the fabricated test geometries are shown in Fig. 2.

3.3. Machining of the structures, in-process strain measurement and post-process deformation detection

The geometrical properties of the builds, the removed material layers i with the induced stress shift and the measured deformation in the yz-Plane are summarized in Fig. 3. The middle longitudinal stress $\sigma_{m,i}$ in layer i before its removal and the stress shift (characterized by $S_{1,i}$ and $S_{2,i}$) are oriented on the nomenclature derived in [16]. As the dominant residual stresses are assumed in the length direction of the build (y-axis) [6 – 10], the main deformation is measured in the yz-plane by the angle α and the distance w. The effect of cutting operations, which are necessary to produce a functional structure, was investigated as follows. The additively generated titanium walls on their substrate were clamped in an *EROWA* vice, which was mounted on a *Kistler 9257B* dynamometer, see Fig. 4. The builds were clamped replicable by using a limit stop above the middle axes of the dynamometer. On the centre point of the substrate's underside, a linear strain gauge *1-LY47-6/120 (HBM)* was applied. Its measuring direction corresponds to the y-axis in order to detect strain ε_i and resulting stress relief $S_{2,i}$ in build length direction. The setup was assembled in a 4-axis machining centre *Heller MC12.*

The generated walls were stepwise milled to reveal the fundamental influence on the total workpiece deformation and stress release depending on the milling position and the varying DED-process. The tool parameters, tool path and cutting parameters are described in Fig. 4. Each material layer i was milled in four work interventions a_e in order to avoid severe tool wear. Due to the wavy surface of the deposit the contact conditions of the 1st and 4th a_e vary slightly in each layer. The

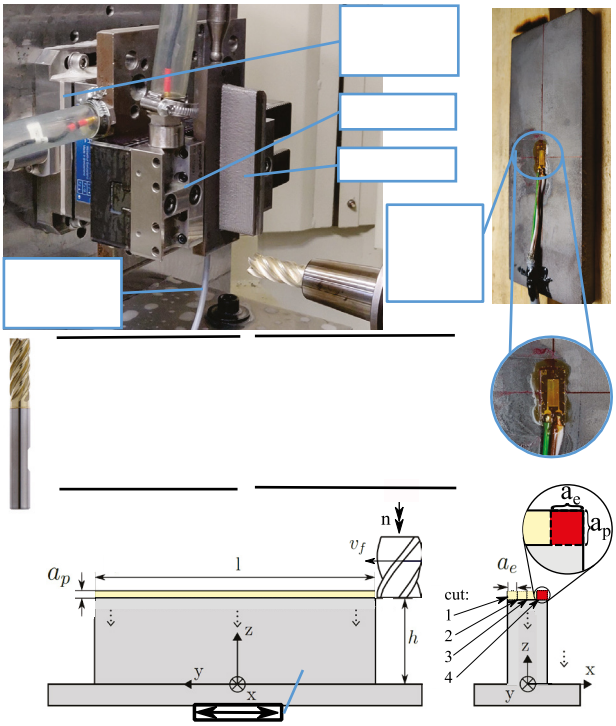

Fig. 4. Experimental setup and procedure of cutting operation.

deposit was completely removed. Each build had a slightly different number of removed layers depending on its fractionally variating height h.

The strain gauge and dynamometer integration allowed for in-process measurement during milling. The strain ε_i was measured through the detection of the voltage drop in the strain gauges using a *Wheatstone* quarter bridge of a *NI-9235 (National Instruments)* measurement module. The strain ε_i was measured in the clamped state to detect stress releases and because clamping forces are assumed significantly lower than stress release deformation forces. The dominant residual stresses of the builds were assumed in deposit length direction (y) and through flood lubrication, no significant material heating was expected. Thus, *Hooke's* law was applied to calculate the yielding stress $S_{2,i}$ at substrate bottom after each material layer removal with E_{Ti64} as *Young's modulus* of the Ti-6Al-4V alloy with the value of 110 GPa in Eq. 1 [17].

$$S_{2,i} = E_{Ti64} \cdot \epsilon_i \quad (1)$$

The tool path went along the coordinate system of the build and the dynamometer, which offered a direct extraction of the cutting forces F_f, F_{fN} and F_P. All in-process signals were edited with the software DIAdem and MATLAB.

Additionally, after each removed layer, a post-process deflection measurement was carried out in order to determine the angle α and distance w. They were obtained in optical measurements with the *Olympus SZX10* microscope. The values were used for the later described evaluation of the initial residual stress state, shown in Fig. 5.

4. Results of the machining process

Fig. 6 presents the stress release at the substrate bottom for each build depending on the wall height h_i. A clear dependence

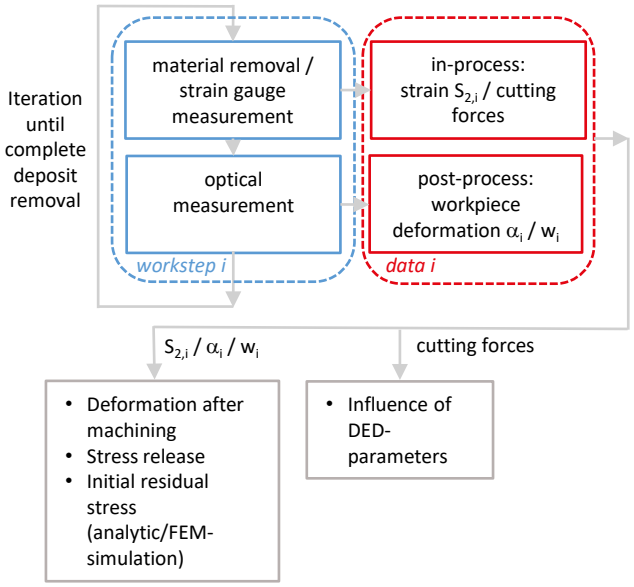

Fig. 5. Iterative workflow for machining of the builds.

on heat treatment and wall height is evident. The not heat-treated build shows very high stress releases, which validated the necessity of the current state-of-art heat treatment requirements. The final sharp bend at the curve of *B1* is due to a lower s_i (and the corresponding a_p) of the final removed deposit layer. The scale-up in 6b displays that the heat-treated builds also induce (low) residual stresses after material removal near the substrate. Here, a tendency is visible that heat treatment in clamped condition leads to lower stress release after material removal and hence lower residual stresses. Each build shows the same behaviour of higher stress release after machining close to substrate.

Fig. 7 confirms the above-described results. Values of the deflection w of the substrate change significantly for the not heat-treated build *B1*. Additionally, cutting forces analysis is presented in Fig. 8. Cutting forces at material removals at similar geometric cutting conditions in close distance from the substrate were compared to minimise material stiffness and hence deflection influence of the measurement. It must be noted that the temporal order of the machining differs from the build number order, which permits the evaluation of the tool wear influence. The result is proved to be significantly influenced by tool wear, as only one tool was used during the experiments and a distinct rise in the resulting cutting force from F_f, F_{fN} and F_P is visible.

5. Evaluation of part deformation and derivation of initial residual stress state

5.1. Methodology

The calculation of the initial residual stress state is based upon stress shift model introduced in [16], assuming a simplified elastic material behavior. Here, the link between residual stress state of the build, material removal in layers, part deformation, stiffness change and stress shift are presented. The stresses induced through the cutting process are neglected,

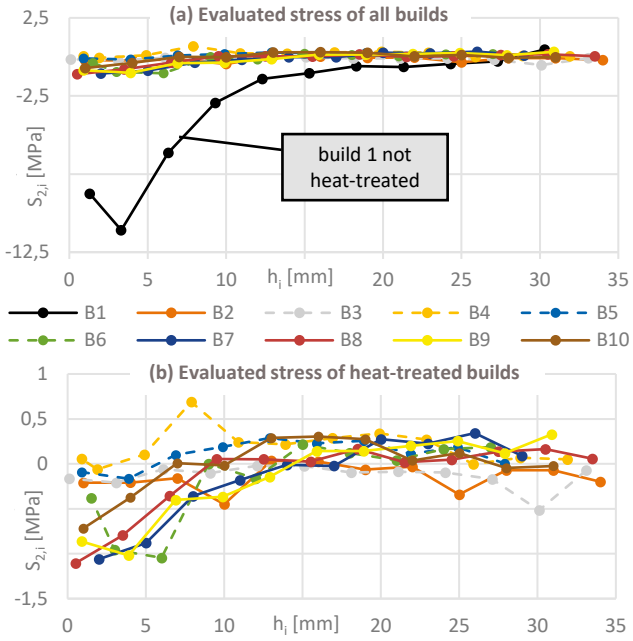

Fig. 6. Stress release at substrate bottom after material removal (dashed / solid lines: heat treatment with / without clamping system).

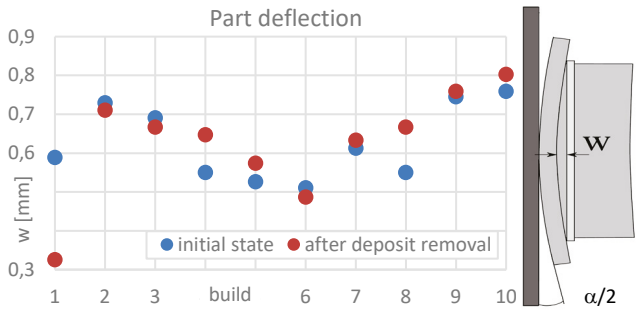

Fig. 7. Part deflection.

as this effect influences only the surface zone of the build. Hence, no significant effect is expected on the entire build deformation. The essential equations (Eq.2/3/4/5) are stated in this study, for a deeper description we refer to the literature [16]. In Eq. 2/3 the relation between the average longitudinal residual stress $\sigma_{m,i}$ in the removed material layer and the evaluated $S_{2,i}$ is incorporated (Fig. 3). Here, the example for the case that the neutral axis (Fig. 3) lies at the substrate top is shown, otherwise a case-by-case analysis was made. Eq. 4/5 state that the avg. stress $\sigma_{y,i,j}$, which is present in layer j after removal of layer i, consists of the initial avg. residual stress $\sigma_{y,j}$ in layer j and the superposition of induced stresses $S_{y,i,j}$ in layer j resulting from stress release after removal of layers i.

The reverse-iterative FEM-simulation of the initial residual stress state after the material removal is described in Fig. 9. The measured strain $\Delta\varepsilon_i$ was used as input for the analytical calculation of equivalent forces $F_{i,eq}$ which induce the strain $\Delta\varepsilon_i$ regarding the geometric properties and assuming the elastic material model. In the next step, $F_{i,eq}$ were applied on the FE-structure of the remaining build. The simulated stresses in the nodes $n_{s,j}$ were used to calculate the mean residual stress in the length direction $\sigma_{FEM,y,j}$ by superposition after each iteration and averaging the result, see Fig. 9. For the analytical and the FEM-

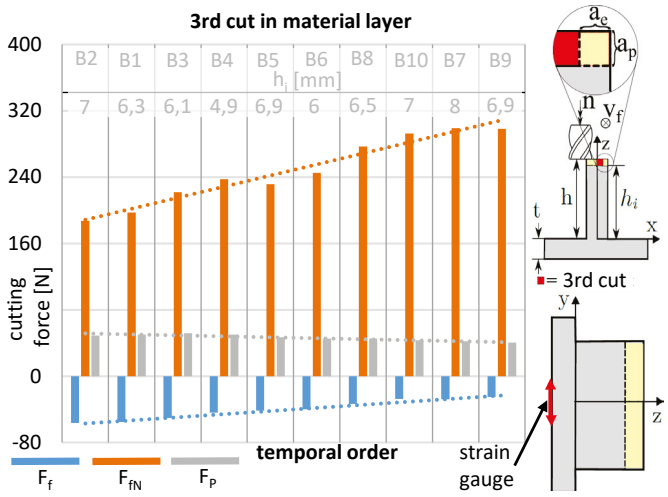

Fig. 8. Cutting forces.

$$\sigma_{m,i} \cdot s_i \cdot d - \frac{S_{1,i} \cdot e_{i,1}}{2} d + \frac{S_{2,i} \cdot e_{i,2}}{2} b = 0 \quad (2)$$

$$S_{1,i} = \frac{S_{2,i}}{e_{2,i}} \cdot e_{1,i} \quad (3)$$

$$\sigma_{y,i,j} = \sigma_{y,j} - \sum_{k=1}^{i} S_{y,k,j} \quad (4)$$

$$S_{y,i,j} = \frac{\sigma_{m,i}}{e_{1,i}} \left[e_{1,i} - \left(j - i + \frac{1}{2} \right) \cdot s_i \right] \quad (5)$$

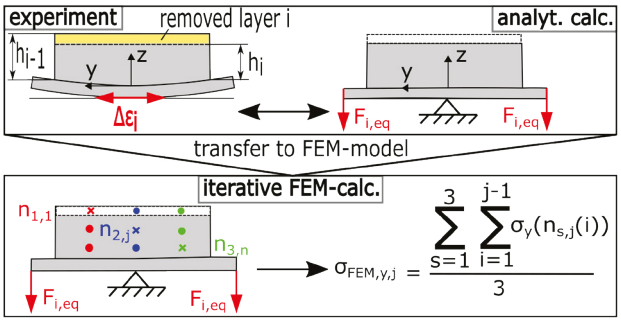

Fig. 9. FEM-simulation of the initial residual stress state.

model the unloaded, symmetrical build with a fixed bearing at the substrate bottom line at $y = 0$ was assumed, as only the difference values are relevant in the iterative workflow. The FEM-simulation was carried out with the software *Inventor 2022* using 3D-tetrahedral elements.

5.2. Results

The summarized results of the analytical and FEM-based initial residual stresses are presented in Fig. 10, where the initial residual stress of each build, averaged for each removed material layer, is plotted versus h_m. Fig 10a reveals that in several heat-treated parts only a rest of residual stresses remain in the first deposited layers, close to the substrate. By the majority this occurs in parts, which were not clamped during the heat treatment. The not-heat-treated build shows significant residual stresses, especially in the layers near the substrate, Fig. 10b.

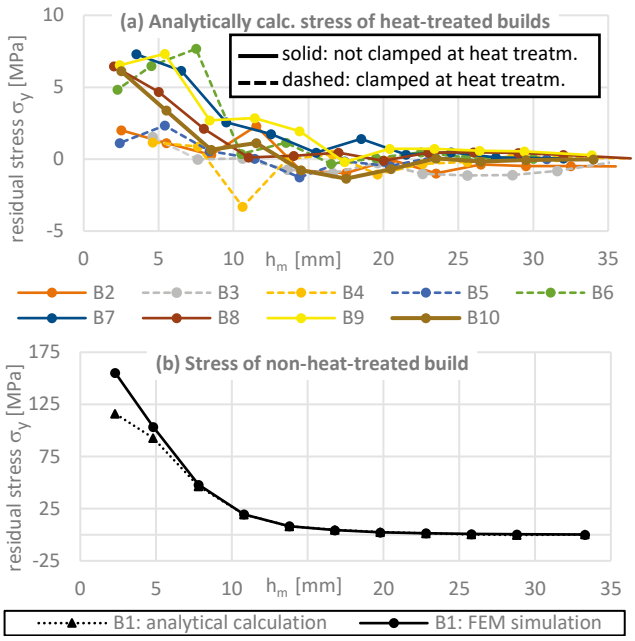

Fig. 10. Initial residual stress states of the builds.

The applied analytical and simulation-based initial stress calculation show mostly identical results, only in the last iteration step these differ. This is supposedly due to numerical inaccuracy and the limitation of the used elastic material model. The results suggest that the predominant residual stresses occur close to the substrate, which indicates that material removal close to the substrate plate must be carefully considered with regard to the precision and stress state of the finished part.

6. Conclusion and outlook

In this experimental work, various Ti-6Al-4V wall geometries, each fabricated with different DED-process strategies were investigated for their residual stress state. For this, the generated structures were machined, and the induced strains were measured during the process with strain gauges. The part deflections were identified through optical measurement after the machining process. The results were then used for a reversed analytical and FEM-based initial residual stress calculation. Both approaches showed similar results and revealed the presence of high residual stresses in the non-heat-treated build and remaining stresses in heat-treated builds. The use of a clamping system during heat treatment tends to induce the lowest residual stresses in the builds. The variation of substrate pre-heating, deposition strategy and dwell-time did not show significant influence on the residual stresses and cutting forces. The calculated initial residual stresses are mainly present in the material layers close to the substrate. This implies that the machining of DED-parts closer to the substrate requires adapted cutting strategies, whereas in distant regions from the substrate, conventional machining strategies are sufficient.

As an extension of this work, effects of variation of build geometry and heat treatment conditions on residual stress states must be studied. Optimized cutting strategies must be identified to achieve a distortion- and residual stress-state -free additive and subtractive process chain for the resource efficient production of lightweight titanium parts.

Acknowledgements

The experimental works and the reported results have been achieved within the framework of the research project *Smart4DED* (13N15038), funded by the German Federal Ministry of Education and Research (BMBF).

References

[1] Liu S, Shin YC. Additive manufacturing of Ti6Al4V alloy: A review. Materials & Design 2019; 164: 107552
[2] Liu Z, He B, Lyu T, Zou Y. A Review on Additive Manufacturing of Titanium Alloys for Aerospace Applications: Directed Energy Deposition and Beyond Ti-6Al-4V. JOM 2021; 6: 1804-1818
[3] Denlinger ER, Michaleris P. Effect of stress relaxation on distortion in additive manufacturing process modeling. Additive Manufacturing 2016; 12: 51-59
[4] Li C, Liu ZY, Fang XY, Guo YB. Residual Stress in Metal Additive Manufacturing. Procedia CIRP 2018; 71: 348–353
[5] Mercelis P, Kruth JP. Residual Stress in Metal Additive Manufacturing. Rapid Prototyping Journal 2006; 12: 254-265
[6] Denlinger ER, Heigel JC, Michaleris P., Palmer TA. Effect of inter-layer dwell time on distortion and residual stress in additive manufacturing of titanium and nickel alloys. Journal of Materials Processing Technology 2015; 215: 123–131
[7] Saboori A, Piscopo G., Lai M., Salmi A, Biamino S. An investigation on the effect of deposition pattern on the microstructure, mechanical properties and residual stress of 316L produced by Directed Energy Deposition. Materials Science and Engineering 2020; 780: 139179
[8] Lu X, Chiumenti M, Cervera M, Li J, Lin X, Ma L, Zhang G, Liang E. Substrate design to minimize residual stresses in Directed Energy Deposition AM processes. Materials & Design 2021; 202: 109525
[9] Lu X, Lin, Xin; Chiumenti, Michele; Cervera, Miguel; Hu, Yunlong; Ji, Xianglin; Ma, Liang; Yang, Haiou; Huang, Weidong. Residual stress and distortion of rectangular and S-shaped Ti-6Al-4V parts by Directed Energy Deposition: Modelling and experimental calibration. Additive Manufacturing 2019; 26: 166–179
[10] Martina F, Roy MJ, Szost BA, Terzi S, Colegrove PA, Williams SW, Withers PJ, Meyer J, Hofmann M. Residual stress of as-deposited and rolled wire+arc additive manufacturing Ti–6Al–4V components. Materials Science and Technology 2016; 32: 1439–1448
[11] Dunbar AJ, Denlinger ER, Gouge MF, Michaleris P. Experimental validation of finite element modeling for laser powder bed fusion deformation. Additive Manufacturing 2016; 12: 108–120
[12] Hoennige JR, Colegrove P, Williams S. Analytical Model for Distortion Prediction in Wire + Arc Additive Manufacturing. Materials Research Proceedings 2018; 6: 277-282
[13] D'Alvise L, Chantzis D, Schoinochoritis B, Salonitis K. Modelling of Part Distortion Due to Residual Stresses Relaxation: An Aeronautical Case Study. Procedia CIRP 2015; 31: 447–452
[14] Heigel JC, Phan TQ, Fox JC, Gnaupel-Herold TH. Experimental Investigation of Residual Stress and its Impact on Machining in Hybrid Additive/Subtractive Manufacturing. Procedia Manufacturing 2018; 26: 929-940
[15] Salonitis K, D'Alvise L, Schoinochoritis B, Chantzis D. Additive manufacturing and post-processing simulation: laser cladding followed by high speed machining. The International Journal of Advanced Manufacturing Technology 2016; 85: 2401–2411
[16] Li B, Deng H, Hui D, Hu Z, Zhang W. A semi-analytical model for predicting the machining deformation of thin-walled parts considering machining-induced and blank initial residual stress. The International Journal of Advanced Manufacturing Technology 2020; 110: 139–161
[17] Hoffmann K. Eine Einfuehrung in die Technik des Messens mit Dehnungsmessstreifen. 1st ed. Pfungstadt: Druckerei Drach Pfungstadt; 1987